Wireless Pers Commun (2011) 59:553–570
DOI 10.1007/s11277-010-9924-8

Performance Analysis of a Complex Multicode Tracking Loop in Bandlimited Rayleigh Fading Channels

Nicolas Y.-H. Hsu · Yu T. Su · Yuan-Bin Lin

Published online: 3 February 2010

Abstract This paper presents the root-mean-squared tracking error performance analysis of a class of coherent digital delay-locked loops for multicode direct sequence spread spectrum signals in bandlimited correlated Rayleigh fading channels. In the transmit side, multiple independent PSK-modulated data streams in the in-phase and qudrature phase branches are spread by short mutually orthogonal codes before being further complex spread by a long complex PN code. We assume that the system employs a pilot code channel to assist the receiver's synchronization and channel estimation. The proposed code tracking loop incorporates the pilot-aided channel estimator and derives the timing error from all short-code-spread subchannels. Our analysis takes into account the effects of imperfect channel estimate, correlated frequency selective Rayleigh fading and band-limiting. Numerical results are presented to quantify the impact of the resulting multipath interference within the same code channel and amongst different code channels.

Keywords Code tracking · Complex multicode spreading · Bandlimited fading

1 Introduction

Various coherent and non-coherent pseudonoise (PN) code tracking loops for direct sequence spread spectrum (DD/SS) signal have been investigated and the related theory is well-established [3,4,6,17,18]. Most studies assume a tracking system which generates a timing error signal by comparing the early and late correlator outputs. In [2,5,9,19] use

This work was supported in part by National Science Council of Taiwan under Grant NSC-93-2218-E-009-015.

N. Y.-H. Hsu
Communication Platform R&D Department, ASUSTek Computer Inc., Taipei, Taiwan
e-mail: Nicolas_Hsu@asus.com.tw

Y. T. Su (✉) · Y.-B. Lin
Department of Communications Engineering, National Chiao Tung University, Hsinchu, Taiwan
e-mail: ytsu@mail.nctu.edu.tw

various linear and nonlinear adaptive filters to estimate the timing error. A complicated multipath interference cancellation mechanism in the tracking loop analyzed in [21]. In spite of the structure differences the majority of existing literatures focus on the conventional single-code spread DS/SS or navigation systems. The design of the code tracking loop for a multicode complex spreading scheme like that used by the third generation (3G) CDMA systems [15] is seldom discussed in open literature. A multicode CDMA system often employs orthogonal codes to channelize individual data streams. The composite multiple code channel signal is further spread by a long signature code. Complex code spreading is preferred to as it results in smaller peak-to-average power ratio.

When detecting a waveform that suffers from correlated frequency selective fading, a receiver needs a channel tracker to compensate for the channel distortions in various operations. In particular, the estimated channel phase rotation has to be incorporated into the code tracking subsystem to de-rotate the received baseband phase so that coherent correlation and combining can be performed. Although channel estimator is a part of the code tracking system very few works investigate the effect of channel estimation error. In [14] analyzed the channel estimation error effect on a single-path tracking loop but he did not taking into account the correlation of the fading process. This paper analyzes the performance of a complex delay-locked loop that is designed to take advantage of the multicode structure for tracking a bandlimited multicode DS/SS signal. Besides additive white Gaussian noise (AWGN), we also consider the effects of correlated Rayleigh fading, bandlimiting and imperfect channel estimation. Borio et al. [1] considered a tracking system structure, which is similar to [7] and what we propose here, that combines the timing estimates obtained from both data and pilot channels. Their work, however, assumes an AWGN channel and did not consider the fading and bandlimiting effects.

The rest of this paper is organized as follows. Section 2 introduces the transmitter and channel models, the proposed coherent code tracking loop structure and channel estimator and the associated parameters. In Sect. 3, we present detailed tracking jitter performance analysis. Computer simulation results that validate our analysis is given in Sect. 4. Finally, conclusion is given in Sect. 5.

2 System and Channel Models

2.1 Transmitter Model

Figure 1 shows the transmitter model considered in this paper. Each parallel code channel carries a distinct data stream and is characterized by the short orthogonal spreading code used to provide the orthogonal channelization among different BPSK-modulated data streams, i.e., the PSK symbols carried by the code channels are spread by mutually orthogonal short codes. We assume that the symbol rate at each code channel is $1/T$ symbols/sec, although variable symbol rate transmission is feasible. By defining $\lfloor i \rfloor_M \triangleq$ integer part of i/M, and $|i|_M \triangleq i$ modulus M, $M \triangleq T/T_c$ being the number of chips per short code period, we can express the orthogonal complex spread data sequence $d_{\lfloor i \rfloor_M}$ as

$$d_{\lfloor i \rfloor_M} = d^I_{\lfloor i \rfloor_M} + j d^Q_{\lfloor i \rfloor_M} = \sum_{k \in \Omega_I} G_k d^{(k)}_{\lfloor i \rfloor_M} W^{(k)}_{|i|_M} + j \sum_{\ell \in \Omega_Q} G_\ell d^{(\ell)}_{\lfloor i \rfloor_M} W^{(\ell)}_{|i|_M}, \tag{1}$$

where the subscripts are the time (chip) indices, the parenthized superscripts denote the subchannel number, $\Omega_I = \{I_1, I_2, \ldots, I_m\}$ and $\Omega_Q = \{Q_1, Q_2, \ldots, Q_n\}$ are the index sets for

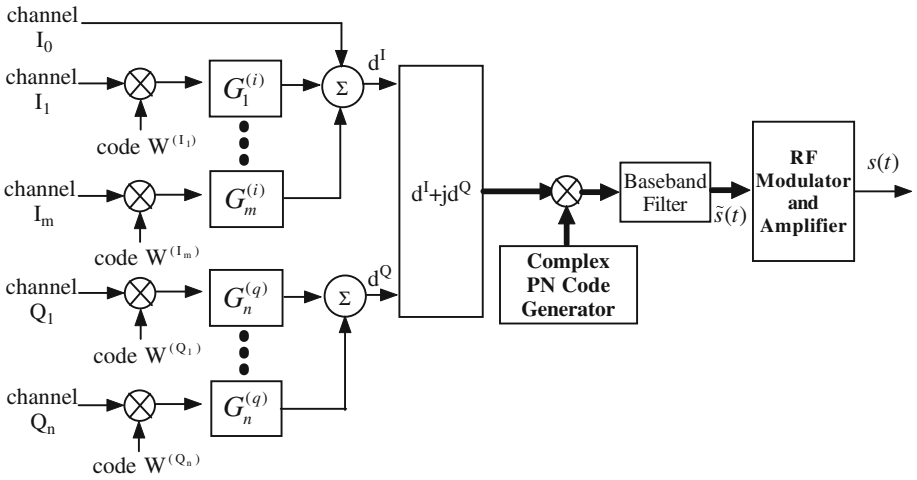

Fig. 1 A complex spread multicode DS/SS transmitter

I- and Q-channels, respectively. G_l, where $l \in \Omega$ and $\Omega = \Omega_I \cup \Omega_Q$, are the channel gains normalized by that of Channel I_0–the pilot channel, i.e., $G_{I_0} = 1$. It should be noted that the pilot does not carry any data, viz., $d^{(I_0)}_{\lfloor i \rfloor_M} = 1 \; \forall \; i$ and uses the code of all ones.

As shown in Fig. 1, the I and Q data streams are further scrambled by a long complex PN code with the same chip rate $1/T_c$. After complex spreading, identical square root raised-cosine (SRRC) baseband filters with impulse and frequency responses $g_T(t)$ and $G_T(f)$ are used to generate waveforms in the I- and Q-channels. The baseband filter and thus the power spectral density (PSD) of the transmitter signal is band-limited to the two-sided bandwidth $B = (1 + \alpha)/T_c$ where $\alpha \in (0, 1)$ is the *rolloff factor*.

The equivalent baseband complex transmitted signal $\tilde{s}(t)$ is a function of the complex-valued data sequence $\{d_{\lfloor i \rfloor_M}\}$ and the spreading sequence $\{c_{\lfloor i \rfloor_N}\}$

$$\tilde{s}(t) = \sum_{i=-\infty}^{\infty} d_{\lfloor i \rfloor_M} c_{|i|_N} g_T(t - iT_c), \tag{2}$$

where T_c is the chip duration and N is the period of the long PN sequence. Since $N \gg M$ and I and Q branches use independent real PN codes, the complex PN sequence $\{c_i\}$ can be regarded as a sequence of independent and identically distributed (i.i.d.) complex random variables with the property

$$\left\langle c_{|i|_N} c^*_{|j|_N} \right\rangle \simeq E\left[c_{|i|_N} c^*_{|j|_N} \right] = \delta[i - j], \tag{3}$$

where $\langle \cdot \rangle$ is the time-averaging operator while $E[\cdot]$ represents the statistical expectation and $*$ denotes the complex conjugate. The Dirac function $\delta[n]$ is defined by

$$\delta[n] \stackrel{\triangle}{=} \begin{cases} 1 & n = 0 \\ 0 & \text{otherwise} \end{cases} \tag{4}$$

2.2 Channel Model and Channel Estimation

We assume that the code tracking loop operates in a slow frequency-selective Rayleigh fading channel, in which the received signal amplitude remains unchanged during a short code

period. To overcome the frequency-selective fading, the so-called *RAKE receiver* is often employed. As in many investigations on multipath fading channels [16] and in industrial standard [15], we use the wide-sense stationary uncorrelated scattering (WSSUS) channel model with the following channel impulse response with respect to the receive timing reference of a RAKE finger

$$\hbar_\varepsilon(\tau;t) = \sum_{l=0}^{L-1} \xi_l(t)\delta[\tau - (\varepsilon T_c + \tau_l)], \tag{5}$$

where L is the number of non-negligible paths, τ_l is the lth path's relative delay and $\xi_l(t)$ is the corresponding complex gain. Without loss of generality, we set $\tau_\ell = 0$ so that $-1/2 < \varepsilon < 1/2$ represents the normalized chip timing error of the tracking loop with respect to the 0th path. Let $\xi(k)$ be the random fading process with the U-shaped Jakes Doppler spectrum [8,12] $S_\xi(f)$ and autocorrelation function $R_\xi(\tau)$ given by

$$\begin{aligned} S_\xi(f) &= \rho_\xi \cdot \begin{cases} \frac{1}{\pi f_d}\left[1-(f/f_d)^2\right]^{-1/2} & \text{if } |f| \le f_d \\ 0 & \text{otherwise,} \end{cases} \\ R_\xi(m) &= \rho_\xi J_0(2\pi f_d \cdot m), \end{aligned} \tag{6}$$

where f_d is the maximum Doppler frequency and ρ_ξ the average power. From (5) and (6), the space-time correlation function of the WSSUS fading process is of the form [12]

$$R_\hbar(\tau;m) = \sum_{l=0}^{L-1} R_{\xi_l}(m)\delta(\tau - \tau_l), \tag{7}$$

where m indicates the time difference.

The receiver needs a channel estimator for RAKE-combining and to compensate for the phase rotation. The optimal filter for estimating the fading process $\{\xi(k)\}$ with known PSD $S_\xi(f)$ in the presence of background noise with PSD $S_n(f)$ is a *Wiener filter* which has the frequency response given by $S_\xi(f)/[S_\xi(f) + S_n(f)]$ [20]. In most case, the Doppler spectrum is unknown or may change with time. As $\{\xi(k)\}$ is a low-pass random process with maximum Doppler frequency f_d, the corresponding optimal Wiener filter is also a low-pass filter. Following the suggestion of [10], we use a low-pass filter with a smooth frequency response up to f_d and a one-sided noise bandwidth greater than f_d to produce the channel estimate.

3 Code Timing Tracking Jitter Analysis

This section provides the mean squared tracking error (jitter) analysis for the code-channel-aided tracking system depicted in Fig. 2 . Before presenting our analysis, it is fitting to discuss the impact of the code tracking error on the bit error rate (BER) performance.

3.1 Impact of Code Timing Jitter on BER Performance

When operating in AWGN channels, the timing jitter σ_ε of a PSK signal is often postulated to follow a Tikhonov probability distribution [11]

$$p(\varepsilon;\sigma_\varepsilon) = \frac{\exp\left[\cos 2\pi\varepsilon/(2\pi\sigma_\varepsilon)^2\right]}{I_0\left[(1/2\pi\sigma_\varepsilon)^2\right]} \tag{8}$$

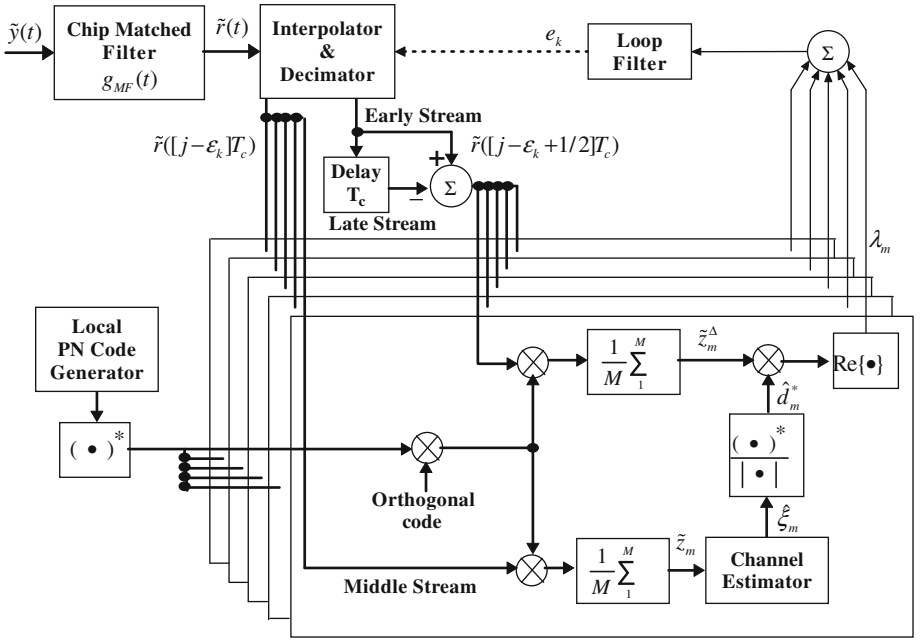

Fig. 2 Block diagram of an all-code-channel-aided coherent PN code tracking loop

For the simplest case when only a single code channel is active, the resulting conditional BER performance, given a fixed code chip offset ε and i.i.d. data source, can be approximated by

$$P_b(e|\varepsilon) \approx \frac{1}{2}Q\left(\sqrt{\frac{2E_b}{N_0}}\right) + \frac{1}{2}Q\left(\sqrt{\frac{2E_b}{N_0}}\,\frac{\langle R_c(|\varepsilon|)\rangle}{M}\right) \tag{9}$$

where $Q(x) \stackrel{def}{=} 1/(\sqrt{2})\int_x^\infty e^{-z^2/2}dz$ and $\langle R_c(z)\rangle$ is the average partial autocorrelation function of the combined short and long codes.[1] The average BER is to be obtained by averaging $P_b(e|\varepsilon)$ over the Tikhonov-distributed ε, i.e.,

$$P_b(e) = \int P_b(e|\varepsilon)\,p(\varepsilon;\sigma_\varepsilon)d\varepsilon \tag{10}$$

For a RAKE receiver operating in a multipath fading channel, the average partial autocorrelation function in (9) should be replaced by that of the combined multiple short codes and long complex code. Furthermore, E_b/N_0 should be replaced by $\xi^2(E_b/N_0)$, where ξ is the RAKE-combined instantaneous signal amplitude, and $P_b(e)$ is to be obtained by taking average with respect to both ξ^2 and ε, assuming slowly flat-fading over at least a bit (symbol) duration. The associated steady state tracking error distribution in such an environment is difficult to analyze. But for the special case when the fading amplitude can be modelled as a Gaussian process whose PSD bandwidth is much wider than that of the tracking loop, Ohlson [13] had obtained a closed-form expression. More detailed analysis and discussion are beyond the scope of this paper but it is safe to conclude that the estimated performance degradation due to code timing jitter alone is insignificant if $\sigma_\varepsilon < 0.05$.

[1] Since the $N \gg M$, the correlation is over a small portion (partial) of the long PN code period, and the average operator $\langle\cdot\rangle$ is thus taken over all possible M-chip segment of the combined code.

3.2 Analysis of Various Correlator Outputs

Now consider the system shown in Fig. 2 in which the received signal is first down-converted to baseband and the resulting quadrature components are filtered by the chip matched filter whose impulse response is $g_{MF}(t) = (1/T_c)g_T^*(-t)$. The filter output can be written as

$$\begin{aligned}\tilde{r}(t) &= \{\tilde{s}(\tau) \otimes \hbar_\varepsilon(\tau; t)|_{\tau=t} + \tilde{w}(t)\} \otimes g_{MF}(t) \\ &= \sum_{i=-\infty}^{\infty} d_{\lfloor i \rfloor_M} c_{|i|_N} \sum_{l=0}^{L-1} \xi_l(t) g\left(t - [\varepsilon T_c + \tau_l] - iT_c\right) + \tilde{n}(t), \end{aligned} \tag{11}$$

where $g(t) \stackrel{\triangle}{=} g_T(t) \otimes g_{MF}(t)$ is the raised cosine function [16], $G(f) = (1/T_c)|G_T(f)|^2$ and $\otimes$ denotes the convolution operator. Since $\tilde{\omega}(t) \stackrel{\triangle}{=} \omega_c(t) + j\omega_s(t)$ is a complex baseband AWGN process whose quadrature components are uncorrelated, zero mean Gaussian processes with two-sided power spectral density (PSD) $S_w(f) = N_0/2P$, P being the IF signal power, the PSD of the noise component, $\tilde{n}(t) = \tilde{\omega}(t) \otimes g_{MF}(t)$, becomes $S_n(f) = N_0 G(f)/(2P)$.

We assume that code acquisition has been accomplished such that the chip timing offset is within $\pm 1/2$ chip. The filter output is over-sampled by an A/D converter and the sampled sequence is forwarded to an interpolator filter. The interpolator together with the decimator are controlled by the chip timing error signal to generate two parallel one sample/chip streams called the middle stream and the early stream, respectively. The operation of the ideal interpolator and decimator resembles that of a down-sampler. Hence, the generation of the middle stream $\tilde{r}_j$ and the early stream $\tilde{r}_{j+1/2}$ is equivalent to sampling $\tilde{r}(t)$ at $t_j = jT_c$ and $t_{j+1/2} = (j + 1/2)T_c$, respectively, i.e.,

$$\tilde{r}_k = \sum_{i=-\infty}^{\infty} d_{\lfloor i \rfloor_M} c_{|i|_N} \sum_{l=0}^{L-1} \xi_{l,k} g([k - i - \varepsilon]T_c - \tau_l) + \tilde{n}_k, \tag{12}$$

where $k = j$ or $k = j + 1/2$, $\xi_{l,k}$ and $\tilde{n}_k$ refer to the sampled version of the complex fading factor and the noise component. Figure 2 depicts a detailed block diagram of the proposed complex DS/SS digital DLL (DDLL) that is similar to an extension of that discussed in [17].

The late sample stream $\tilde{r}_{j-1/2}$ is simply one-chip delayed version of the early sample stream $\tilde{r}_{j+1/2}$. They are complex multiplied by the conjugate of the local generated complex PN code then separated by distinct short code correlators. Only the pilot channel is used for tracking and channel estimation. The corresponding despread outputs at the early-late-difference and middle branches are thus given by

$$\tilde{z}_m^{\Delta} = \frac{1}{M} \sum_{j=mM}^{(m+1)M-1} \left(\tilde{r}_{j+1/2} - \tilde{r}_{j-1/2}\right) c_{|j|_N}^*, \tag{13}$$

$$\tilde{z}_m = \frac{1}{M} \sum_{j=mM}^{(m+1)M-1} \tilde{r}_j c_{|j|_N}^*. \tag{14}$$

3.3 First- and Second-Order Statistics

The estimate $\hat{\xi}_m$ of the complex channel gain factor is obtained by passing the quadrature components of the despread samples $\tilde{z}_m$ through a pair of (identical) low-pass filters. The

resulting estimate can be expressed as

$$\hat{\xi}_m = \tilde{z}_m \otimes h_m^e, \tag{15}$$

where h_m^e is the impulse response of the channel estimation filter. The early-late difference $\tilde{z}_m^{\Delta}$ is multiplied by the conjugate of the estimated phasor to obtain the error signal

$$\lambda_m = \Re\left\{\tilde{z}_m^{\Delta}\frac{\hat{\xi}_m^*}{|\hat{\xi}_m|}\right\}. \tag{16}$$

The sum of λ_m is lowpass filtered by an integrated-and-dump filter with an integration period of KM chip intervals. The kth loop filter output e_k is then used to control the interpolator filter output so that the equivalent sampling instant is updated every KMT_c seconds via $\varepsilon_{k+1} = \varepsilon_k + \mu e_k$, where μ is the sensitivity of the loop filter.

The average loop error characteristic is defined by

$$\eta(\varepsilon) \triangleq \langle E\{e_k|\varepsilon_k = \varepsilon\ \forall\, k\}\rangle, \tag{17}$$

which is related to the *normalized S-curve* of the loop via $S(\varepsilon) \triangleq \frac{1}{A}\eta(\varepsilon)$, where $A \triangleq \left.\frac{d\eta(\varepsilon)}{d\varepsilon}\right|_{\varepsilon=0}$, the slope at $\varepsilon = 0$ of the loop error characteristic, is used for normalization such that $\left.\frac{dS(\varepsilon)}{d\varepsilon}\right|_{\varepsilon=0} = 1$. For the tracking loop shown in Fig. 2, we define the noise sequence $\{N_k\}$, $N_k \triangleq -\mu[e_k - \eta(\varepsilon_k)]$, so that the loop update equation can be expressed as $\varepsilon_{k+1} = \varepsilon_k - \mu AS(\varepsilon_k) + N_k$. Invoking the linear approximation at neighborhood of $\varepsilon = 0$, $S(\varepsilon) \approx \varepsilon$, we obtain $\varepsilon_{k+1} = (1-\mu A)\varepsilon_k + N_k$. Letting $a = 1-\mu A < 1$, we rewrite the update equation as $\varepsilon_{k+1} = a\varepsilon_k + N_k$.

From (17), we have $\langle E\{N_k\}\rangle = -\mu\langle E\{e_k - \eta(\varepsilon_k)\}\rangle = 0$. To simply the analysis, we assume that $\{N_k\}$ is a sequence of uncorrelated and identical distributed random variables, i.e.,

$$\begin{aligned}\langle E\{N_k N_{k+n}\}\rangle &= 0 \qquad \text{if } n \neq 0,\\ \langle Var\{N_k\}\rangle &= \left\langle E\{N_k^2\}\right\rangle.\end{aligned} \tag{18}$$

After some algebra, we obtain

$$\langle E\{\varepsilon_k\}\rangle = \left\langle E\left\{a^k\varepsilon_0 + a^{k-1}N_0 + a^{k-2}N_1 + \cdots + N_{k-1}\right\}\right\rangle = a^k\varepsilon_0 \tag{19}$$

and

$$\begin{aligned}\left\langle E\{\varepsilon_k^2\}\right\rangle &= a^2\left\langle E\{\varepsilon_{k-1}^2\}\right\rangle + 2a\langle E\{\varepsilon_{k-1}N_{k-1}\}\rangle + \left\langle E\{N_{k-1}^2\}\right\rangle\\ &= a^{2k}\varepsilon_0^2 + \left\langle E\{N_{k-1}^2\}\right\rangle\frac{1-a^{2k}}{1-a^2}.\end{aligned} \tag{20}$$

As expected, ε_k is asymptotically independent of ε_0, and ε_k and ε_{k+n} are almost uncorrelated if $|n| \gg 1$. (19) and the properties of $\{N_k\}$ imply that the steady-state timing error is given by

$$\sigma_\varepsilon^2 \triangleq \frac{\left\langle E\{N_k^2\}\right\rangle|_{\varepsilon=0}}{1-a^2}, \tag{21}$$

where the average power of the zero-mean loop noise is

$$\left\langle E\{N_k^2\}\right\rangle = \mu^2\left[E\{e_k^2\} - \eta^2(\varepsilon)\right]. \tag{22}$$

To evaluate $\langle E\{e_k^2\}\rangle$ we first notice that both $\tilde{z}_m^{\Delta}$ and $\hat{\xi}_m$ are complex Gaussian distributed. Define

$$\tilde{z}_m^{\Delta} = x_1 + jx_2 = r_1 e^{j\phi_1}, \qquad \hat{\xi}_m = x_3 + jx_4 = r_2 e^{j\phi_2}. \tag{23}$$

Applying the general Rayleigh fading process assumption, i.e., the in-phase and quadrature phase processes are mutually independent and identically distributed (i.i.d.), we have

$$E\{x_1 x_2\} = E\{x_1 x_2\} = 0 \tag{24}$$

$$E\{{x_1}^2\} = E\{{x_2}^2\} = E\{|\tilde{z}_m^{\Delta}|^2\}/2 \stackrel{\Delta}{=} {\sigma_1}^2 \tag{25}$$

$$E\{{x_3}^2\} = E\{{x_4}^2\} = E\{|\tilde{\xi}_m^{\Delta}|^2\}/2 \stackrel{\Delta}{=} {\sigma_2}^2 \tag{26}$$

$$E\{x_1 x_3\} = E\{x_2 x_4\} \stackrel{\Delta}{=} \mu_1 \tag{27}$$

$$E\{x_1 x_4\} = -E\{x_2 x_3\} \stackrel{\Delta}{=} \mu_2. \tag{28}$$

By transforming the rectangular coordinate (x_1, x_2, x_3, x_4) into the polar coordinate $(r_1, r_2, \phi_1, \phi_2)$ and making the change of variables, $\psi = \phi_1 - \phi_2$, we obtain

$$p(r_1, r_2, \psi) = \frac{r_1 r_2}{2\pi\sigma_1^2\sigma_2^2(1-\rho^2)} \cdot \exp\left\{-\frac{1}{2(1-\rho^2)}\left[\frac{r_1^2}{\sigma_1^2} + \frac{r_2^2}{\sigma_2^2} - 2\frac{r_1 r_2}{\sigma_1\sigma_2}(\rho_1 \cos\psi - \rho_2 \sin\psi)\right]\right\}, \tag{29}$$

where $\rho_1 \stackrel{\Delta}{=} \mu_1/(\sigma_1\sigma_2)$, $\rho_2 \stackrel{\Delta}{=} \mu_2/(\sigma_1\sigma_2)$, and $\rho \stackrel{\Delta}{=} \sqrt{\rho_1^2 + \rho_2^2}$.

Substituting (23) into (16), we obtain $\lambda_m = r_1 \cos\psi$. In *"Appendix A"* we prove that the corresponding first and second moments are

$$E\{\lambda_m\} = \int_{-\pi}^{\pi}\int_0^{\infty}\int_0^{\infty} (r_1\cos\psi)\, p(r_1, r_2, \psi)\, dr_1 dr_2 d\psi = \frac{\mu_1}{\sigma_2}\sqrt{\frac{\pi}{2}}, \tag{30}$$

$$E\{\lambda_m^2\} = \int_{-\pi}^{\pi}\int_0^{\infty}\int_0^{\infty} (r_1\cos\psi)^2\, p(r_1, r_2, \psi)\, dr_1 dr_2 d\psi = \sigma_1^2(1 + \rho_1^2 - \rho_2^2). \tag{31}$$

The detail expression for ${\sigma_1}^2$, ${\sigma_2}^2$ and μ_1 are given in *"Appendix B"*.

Assuming λ_m's are i.i.d. random variables with first and second moments given by

$$E\{e_k\} = E\{\lambda_m\}, \qquad Var\{e_k\} = \frac{1}{K} Var\{\lambda_m\}, \tag{32}$$

where K is the accumulation interval, and substituting (32) into (22), we obtain

$$\langle E\{N_k^2\}\rangle = \frac{\mu^2}{K}\sigma_1^2\left[1 + \rho_1^2\left(1 - \frac{\pi}{2}\right)\right]. \tag{33}$$

Substituting it into (21), replacing a by $1 - \mu A$, and taking the square root, we then obtain the chip timing jitter

$$\sigma_\varepsilon = \frac{1}{A}\sqrt{\frac{2B_L T_c}{K}\sigma_1^2\left[1 + \rho_1^2\left(1 - \frac{\pi}{2}\right)\right]}, \tag{34}$$

where the normalized loop bandwidth is

$$B_L T_c = \frac{\mu A}{2(2 - \mu A)}. \tag{35}$$

4 Simulation Results and Discussion

This section reports some numerical behaviors of the proposed combined channel estimate and coherent code tracking subsystem. These results are obtained by using both the derived analytic expressions and computer simulations based on the following system parameters:

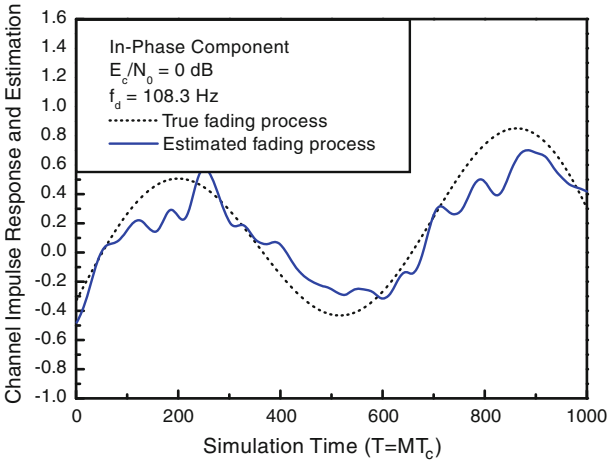

Fig. 3 Comparison of the trajectories of the true and estimated in-phase amplitude fading processes

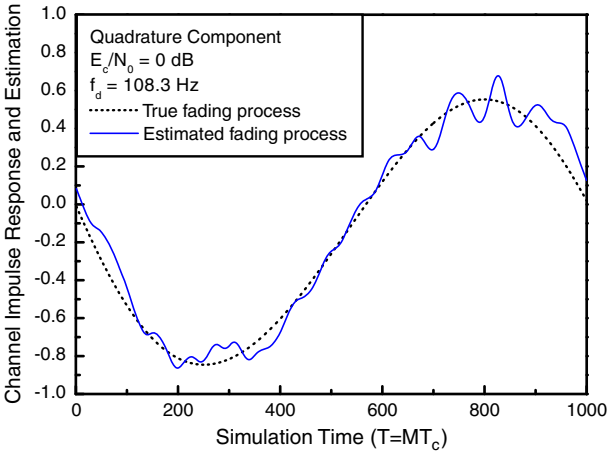

Fig. 4 Trajectories of the true and estimated quadrature-phase amplitude fading processes

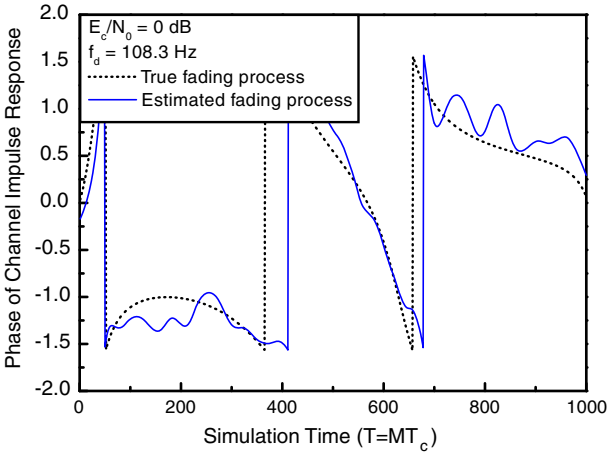

Fig. 5 Trajectories of the true and estimated phases of the correlated fading process

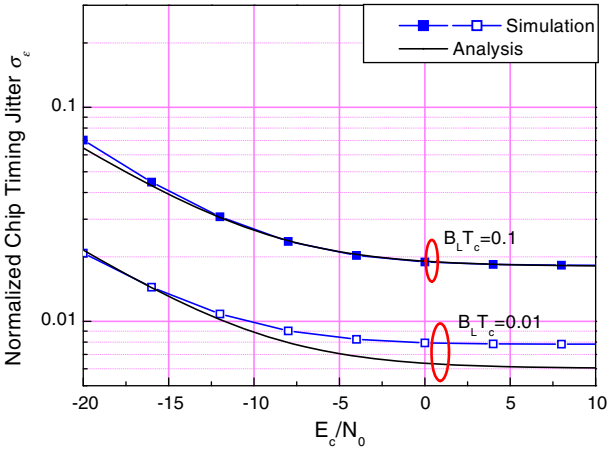

Fig. 6 Normalized timing jitter performance predicted by analysis and simulation in a bandlimited correlated fading channel; $B_L T_c = 0.1$ and $B_L T_c = 0.01$

- The generator polynomial for the long code:

$$p_L(x) = 1 + x^2 + x^3 + x^5 + x^6 + x^7 + x^{10} + x^{16} + x^{17} + x^{18} + x^{19} + x^{21} + x^{22} + x^{25} + x^{26} + x^{27} + x^{31} + x^{33} + x^{35} + x^{42}$$

- Chip rate: $R_c = 1/T_c = 1.2288$ Mcps
- Spreading factor: $M = 16$
- Maximum Doppler frequency: $f_d = 108.3$ Hz
- E_c/N_0: Pilot channel's chip energy to noise power level ratio
- Number of code channels: 3 channels for the I-branch and 2 channels for the Q-branch
- Power vector $\mathbf{P}$: $\mathbf{P} \triangleq [P_{0_I}\ P_{1_I}\ P_{2_I}\ P_{1_Q}\ P_{2_Q}] = [1\ 1\ 1\ 2\ 5]$

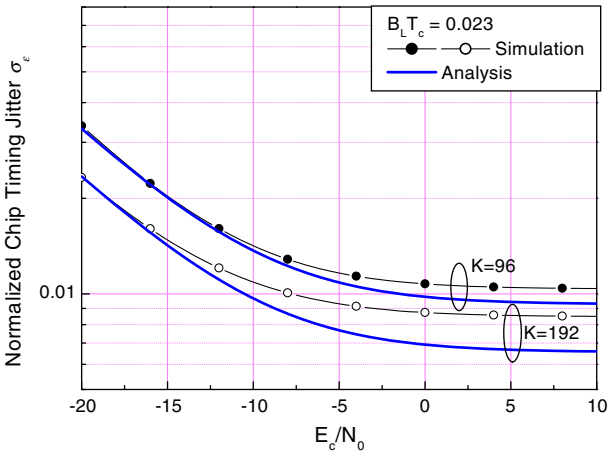

Fig. 7 Effect of the filter window size on the normalized timing jitter performance predicted by analysis and simulation in a bandlimited correlated fading channel

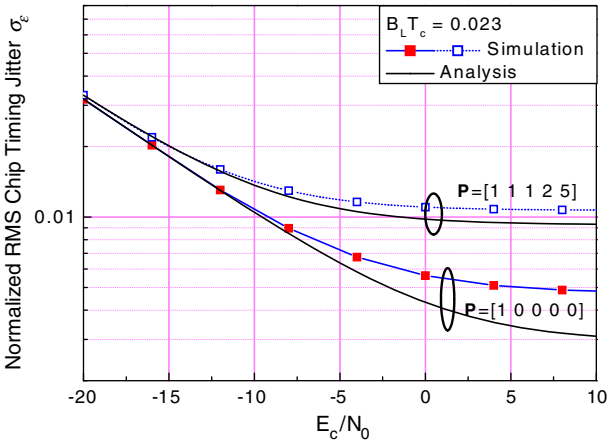

Fig. 8 Effect of self-interference on the code tracking performance in a correlated fading channel

We use a two-ray Rayleigh fading model with the fading process of each ray derived from Jakes' two-dimensional isotropic scattering model. To estimate the channel gain factor, a forth-order Butterworth low-pass filter with sampling frequency 76.8 kHz and cutoff frequency 1 kHz is used.

Figures 3 and 4 compare the estimated trajectories of the magnitudes of in-phase and quadrature-phase channel fading processes. Figure 5 compares the true and estimated fading phase trajectories and indicates that there is a delay between simulated and estimated phase trajectories which is caused by the low-pass filtering process and is inverse proportional to the filter bandwidth. The estimate phase delay will impact the tracking performance.

Figures 6 and 7 compare the simulation and analytical results for various normalized loop bandwidths, $B_L T_c$, and filter window size K. As is expected, the jitter performance is improved by decreasing the loop bandwidth or increasing the filter window size. The increase of the window size enhances the correlation of the estimated error indicator samples λ_m while for a fixed Doppler shift the increase of the normalized loop bandwidth tends to decrease the

correlation. The increased correlation on λ_m leads to our overestimate on the timing jitter especially when E_c/N_0 is high.

The existence of a floor in each jitter performance curve is due to the self-interference caused by data channels. Bandlimiting leads to a non-negligible chip pulse extension in the time domain and thus the orthogonality among various orthogonal codes is destroyed, creating non-zero cross-correlation between the pilot code and other channelization codes. Figure 8 examines the effect of self-interference. We compare the timing jitter performance for the case when five code channels are all activated with that when only the pilot channel is used. Imperfect channel estimation also enhances the self-interference effect which dominates the jitter performance at higher E_c/N_0.

5 Conclusion

We have investigated the behavior of a coherent digital delay-locked loop for tracking bandlimited complex DS/SS signals in slow frequency-selective Rayleigh fading channels and analyzed the corresponding root mean square tracking jitter performance. The code tracking loop uses both pilot and data channels and incorporates a suboptimal channel estimator to compensate for the fading effect.

Simulation results indicate that our analysis does offer accurate performance prediction. Both our analysis and simulation results pointed out that, for multicode complex PN code tracking loop, the bandlimiting and multipath effects destroy the orthogonality of the short orthogonal spreading codes and induces self-interference among code channels, resulting in an irreducible tracking jitter. Interference cancellation is therefore, called for to remove this performance lower bound.

Appendix A Derivation of the First Two Moments of λ_m

Invoking (29) and the changes of variables $r_1' = \frac{r_1}{\sigma_1\sqrt{1-\rho^2}}$ and $r_2' = \frac{r_2}{\sigma_2\sqrt{1-\rho^2}}$, we obtain

$$\begin{aligned} E\{\lambda_m\} &= \int_{-\pi}^{\pi}\int_{0}^{\infty}\int_{0}^{\infty}(r_1\cos\psi)\,p(r_1,r_2,\psi)\,dr_1dr_2d\psi \\ &= \frac{\sigma_1(1-\rho^2)^{3/2}}{2\pi}\int_{0}^{\infty}\int_{0}^{\infty}\int_{-\pi}^{\pi} r_1^2 r_2\cos\psi \\ &\quad\cdot\exp\left\{-\frac{1}{2}\left[r_1^2+r_2^2-2r_1r_2(\rho_1\cos\psi-\rho_2\sin\psi)\right]\right\}d\psi dr_1dr_2 \end{aligned} \tag{A.1}$$

The substitutions $x = r_1\cos\psi$ and $y = r_1\sin\psi$ then lead to

$$\begin{aligned} E\{\lambda_m\} &= \frac{\sigma_1(1-\rho^2)^{3/2}}{2\pi}\int_{0}^{\infty}\int_{-\infty}^{\infty}\int_{-\infty}^{\infty} x r_2 \\ &\quad\cdot\exp\left\{-\frac{1}{2}\left[x^2+y^2+r_2^2-2\rho_1r_2x+2\rho_2r_2y\right]\right\}dydxdr_2 \end{aligned}$$

$$= \sigma_1(1-\rho^2)^{3/2} \int_0^{\infty} r_2^2 \exp\left\{-\frac{1}{2}(1-\rho^2)r_2^2\right\} dr_2$$

$$= \frac{\mu_1}{\sigma_2}\sqrt{\frac{\pi}{2}} \tag{A.2}$$

Similarly, we can shown

$$\begin{aligned}
E\{\lambda_m^2\} &= \int_{-\pi}^{\pi}\int_0^{\infty}\int_0^{\infty} (r_1\cos\psi)^2 p(r_1, r_2, \psi) dr_1 dr_2 d\psi \\
&= \frac{1-\rho^2}{2\pi}\int_0^{\infty}\int_0^{\infty}\int_{-\pi}^{\pi} \left(\sigma_1\sqrt{1-\rho^2}r_1\cos\psi\right)^2 r_1 r_2 \\
&\quad \cdot \exp\left\{-\frac{1}{2}\left[r_1^2 + r_2^2 - 2r_1 r_2(\rho_1\cos\psi - \rho_2\sin\psi)\right]\right\} d\psi dr_1 dr_2 \\
&= \frac{\sigma_1^2(1-\rho^2)^2}{\sqrt{2\pi}}\int_0^{\infty}\int_{-\infty}^{\infty} x^2 r_2 \exp\left\{-\frac{1}{2}(x-\rho_1 r_2)^2\right\}\exp\left\{-\frac{1-\rho^2}{2}r_2^2\right\} dx dr_2 \\
&= \frac{\sigma_1^2(1-\rho^2)^2}{\sqrt{2\pi}}\left\{\frac{2\sqrt{\pi}}{4(\frac{1}{2})^{3/2}}\int_0^{\infty} r_2 \exp\left\{-\frac{1-\rho^2}{2}r_2^2\right\} dr_2 + \rho_1^2\sqrt{2\pi}\right. \\
&\quad \left. \times \int_0^{\infty} r_2^3 \exp\left\{-\frac{1-\rho^2}{2}r_2^2\right\} dr_2\right\} \\
&= \sigma_1^2(1+\rho_1^2-\rho_2^2).
\end{aligned} \tag{A.3}$$

Appendix B The Derivation of the Average Autocorrelation Function

Rewrite (14) as $\tilde{z}_m^{\Delta} = E[\tilde{z}_m^{\Delta}] + \{\tilde{z}_m^{\Delta}\} \triangleq \tilde{u}_m^{\Delta} + \tilde{v}_m^{\Delta}$, From (12), we have

$$\tilde{u}_m^{\Delta} = \frac{1}{M}\sum_{j=mM}^{(m+1)M-1}\sum_{i=-\infty}^{\infty} d_{\lfloor i\rfloor_M} c_{|i|_N} c_{|j|_N}^* \sum_{l=0}^{L-1}\xi_{l,m} f_l(j-i-\varepsilon, 1/2) \tag{B.1}$$

$$\tilde{v}_m^{\Delta} = \frac{1}{M}\sum_{j=mM}^{(m+1)M-1}\left(\tilde{n}_{j+1/2} - \tilde{n}_{j-1/2}\right) c_{|j|_N}^* \tag{B.2}$$

where

$$f_l(i, j) \triangleq g([i+j]T_c - \tau_l) - g([i-j]T_c - \tau_l). \tag{B.3}$$

In the slow fading channel, the discrete fading factor, $\xi_{l,m}$, remains unchanged over an orthogonal code period. To derive σ_1^2, σ_2^2 and μ_1, we ought to calculate the correlation of signal components $\tilde{u}_m^{\Delta}$, $\tilde{u}_m$ and noise components $\tilde{v}_m^{\Delta}$, $\tilde{v}_m$.

$$
\begin{aligned}
&\left\langle E[u_m^{\Delta} u_{m-k}^{\Delta *}] \right\rangle \\
&= \frac{1}{M^2} \left\langle E \left[\sum_{j=mM}^{(m+1)M-1} \sum_{i=-\infty}^{\infty} d_{\lfloor i \rfloor_M} c_{|i|_N} c_{|j|_N}^{*} \sum_{l=0}^{L-1} \xi_{l,m} f_l(j - i - \varepsilon, 1/2) \right.\right. \\
&\quad \left.\left. \cdot \left(\sum_{j=(m-k)M}^{(m-k+1)M-1} \sum_{i=-\infty}^{\infty} d_{\lfloor i \rfloor_M} c_{|i|_N} c_{|j|_N}^{*} \sum_{l=0}^{L-1} \xi_{l,m-k} f_l(j - i - \varepsilon, 1/2) \right)^{*} \right] \right\rangle \\
&= \frac{1}{M^2} \sum_{j=mM}^{(m+1)M-1} \sum_{i=-\infty}^{\infty} \sum_{q=(m-k)M}^{(m-k+1)M-1} \sum_{p=-\infty}^{\infty} \left\langle E \left[d_{\lfloor i \rfloor_M} d_{\lfloor p \rfloor_M}^{*} c_{|i|_N} c_{|j|_N}^{*} c_{|p|_N}^{*} c_{|q|_N} \right.\right. \\
&\quad \left.\left. \cdot \sum_{l=0}^{L-1} \sum_{l'=0}^{L-1} \xi_{l,m} \xi_{l',m-k}^{*} f_l(j - i - \varepsilon, 1/2) f_{l'}(q - p - \varepsilon, 1/2) \right] \right\rangle
\end{aligned} \tag{B.4}
$$

From (6) and (7), we obtain the autocorrelation of the fading gain factor:

$$
E \left[\sum_{l=0}^{L-1} \sum_{l'=0}^{L-1} \xi_{l,m} \xi_{l',m-k}^{*} \right] = \sum_{l=0}^{L-1} \rho_{\xi_l} J_0(2\pi f_d k T). \tag{B.5}
$$

Substituting above equation into (B.4) and after some algebra, we obtain

$$
\begin{aligned}
&\left\langle E[u_m^{\Delta} u_{m-k}^{\Delta *}] \right\rangle \\
&= \frac{1}{M^2} \left\{ \sum_{j=0}^{M-1} \sum_{q=-kM}^{(-k+1)M-1} R_d(j-q) \sum_{l=0}^{L-1} \rho_{\xi_l} J_0(2\pi f_d k T) f_l^2(-\varepsilon, 1/2) \right. \\
&\quad \left. + M R_d(0) \delta[k] \sum_{\substack{i=-\infty \\ i \neq 0}}^{\infty} \sum_{l=0}^{L-1} \rho_{\xi_l} J_0(2\pi f_d k T) f_l^2(-i - \varepsilon, 1/2) \right\}
\end{aligned} \tag{B.6}
$$

Similarly, we can show that

$$
\begin{aligned}
&\left\langle E[u_m u_{m-k}^{*}] \right\rangle \\
&= \frac{1}{M^2} \left\langle E \left[\sum_{j=mM}^{(m+1)M-1} \sum_{i=-\infty}^{\infty} d_{\lfloor i \rfloor_M} c_{|i|_N} c_{|j|_N}^{*} \sum_{l=0}^{L-1} \xi_{l,m} g([j - i - \varepsilon] T_c - \tau_l) \right.\right. \\
&\quad \left.\left. \cdot \left(\sum_{q=(m-k)M}^{(m-k+1)M-1} \sum_{p=-\infty}^{\infty} d_{\lfloor p \rfloor_M}^{*} c_{|p|_N}^{*} c_{|q|_N} \sum_{l=0}^{L-1} \xi_{l,m-k} g([p - q - \varepsilon] T_c - \tau_l) \right)^{*} \right] \right\rangle
\end{aligned}
$$

$$= \frac{1}{M^2}\left\{ \sum_{j=0}^{M-1} \sum_{q=-kM}^{(-k+1)M-1} R_d(j-q) \sum_{l=0}^{L-1} \rho_{\xi_l} J_0(2\pi f_d kT) g^2(-\varepsilon T_c - \tau_l) \right.$$

$$\left. + M R_d(0)\delta[k] \sum_{\substack{i=-\infty \\ i\neq 0}}^{\infty} \sum_{l=0}^{L-1} \rho_{\xi_l} J_0(2\pi f_d kT) g^2([-i-\varepsilon]T_c - \tau_l) \right\} \tag{B.7}$$

and

$$\left\langle E[u_m^{\Delta} u_{m-k}^*] \right\rangle$$

$$= \frac{1}{M^2}\left\{ \sum_{j=0}^{M-1} \sum_{q=-kM}^{(-k+1)M-1} R_d(j-q) \sum_{l=0}^{L-1} \rho_{\xi_l} J_0(2\pi f_d kT) f_l(-\varepsilon, 1/2) g(-\varepsilon T_c - \tau_l) \right.$$

$$\left. + M R_d(0)\delta[k] \sum_{\substack{i=-\infty \\ i\neq 0}}^{\infty} \sum_{l=0}^{L-1} \rho_{\xi_l} J_0(2\pi f_d kT) f_l(-i-\varepsilon, 1/2) g([-i-\varepsilon]T_c - \tau_l) \right\} \tag{B.8}$$

The average autocorrelation function of the noise component is derived as follows.

$$\left\langle E[v_m^{\Delta} v_{m-k}^*] \right\rangle$$

$$= \frac{1}{M^2}\left\langle E\left[\sum_{j=mM}^{(m+1)M-1} (\tilde{n}_{j+1/2} - \tilde{n}_{j-1/2}) c_{|j|_N}^* \sum_{j=(m-k)M}^{(m-k+1)M-1} (\tilde{n}_{j+1/2} - \tilde{n}_{j-1/2})^* c_{|j|_N} \right] \right\rangle$$

$$= \frac{1}{M^2}\left\langle \sum_{j=mM}^{(m+1)M-1} \sum_{q=(m-k)M}^{(m-k+1)M-1} E\left[(\tilde{n}_{j+1/2} - \tilde{n}_{j-1/2})(\tilde{n}_{q+1/2} - \tilde{n}_{q-1/2})^* \right] c_{|j|_N}^* c_{|q|_N} \right\rangle$$

$$= \frac{1}{M^2} \sum_{j=mM}^{(m+1)M-1} \sum_{q=(m-k)M}^{(m-k+1)M-1} \left(4\sigma_n^2 \delta[j-q] - 2\sigma_n^2 \delta[j-q-1] - 2\sigma_n^2 \delta[j-q-1] \right)$$

$$\times \left\langle c_{|j|_N}^* c_{|q|_N} \right\rangle$$

$$= \frac{1}{M^2} \sum_{j=mM}^{(m+1)M-1} \sum_{q=(m-k)M}^{(m-k+1)M-1} \left(4\sigma_n^2 \delta[j-q] - 2\sigma_n^2 \delta[j-q-1] - 2\sigma_n^2 \delta[j-q-1] \right) \delta[j-q]$$

$$= \frac{4}{M} \sigma_n^2 \delta[k] \tag{B.9}$$

Similarly, we can verify that $\left\langle E[v_m v_{m-k}^*] \right\rangle = \frac{2}{M}\sigma_n^2 \delta[k]$ and $\left\langle E[v_m^{\Delta} v_{m-k}^*] \right\rangle = 0$. Hence σ_1^2, σ_2^2 and μ_1 are given by

$$\sigma_1^2 = \frac{1}{2}\left\langle E\{|\tilde{z}_m^{\Delta}|^2\}\right\rangle$$
$$= \frac{1}{2M^2}\left\{\sum_{l=0}^{L-1}\rho_{\xi_l}J_0(0)\sum_{j=0}^{M-1}\sum_{q=0}^{M-1}R_d(j-q) + R_d(0)M\sum_{l=0}^{L-1}\rho_{\xi_l}J_0(0)\right.$$
$$\left.\times\sum_{\substack{i=-\infty\\ i\neq 0}}^{\infty} f_l^2(-i-\varepsilon,1/2)\right\} + \frac{2}{M}\sigma_n^2. \tag{B.10}$$

$$\sigma_2^2 = \frac{1}{2}\left\langle E\{|\hat{\xi}_m|^2\}\right\rangle$$
$$= \frac{1}{2}\sum_{\alpha=-\infty}^{\infty}\left\{\left\langle E[u_{m-\alpha}u_m^*] + E[v_{m-\alpha}v_m^*]\right\rangle\right\}\sum_{\beta=-\infty}^{\infty}h^e[\alpha+\beta]h^e[\beta]$$
$$= \frac{1}{2}\sum_{\alpha=-\infty}^{\infty}\left\{\frac{1}{M^2}\sum_{j=0}^{M-1}\sum_{q=\alpha M}^{(\alpha+1)M-1}R_d(j-q)\sum_{l=0}^{L-1}\rho_{\xi_l}J_0(-2\pi f_d\alpha T)g^2(-\varepsilon T_c-\tau_l)\right.$$
$$\left.+\delta[\alpha]R_d(0)\frac{1}{M}\sum_{\substack{i=-\infty\\ i\neq 0}}^{\infty}\sum_{l=0}^{L-1}\rho_{\xi_l}J_0(-2\pi f_d\alpha T)g^2([-i-\varepsilon]T_c-\tau_l)+\delta[\alpha]\frac{2}{M}\sigma_n^2\right\}$$
$$\times\sum_{\beta=-\infty}^{\infty}h^e[\alpha+\beta]h^e[\beta]. \tag{B.11}$$

and

$$\mu_1 = \frac{1}{2}\left\langle E\left[\tilde{z}_m^{\Delta}\hat{\xi}_m^*\right]\right\rangle$$
$$= \frac{1}{2}\sum_{\alpha=-\infty}^{\infty}h^e[\alpha]\left\{\left\langle E[u_m^{\Delta}u_{m-\alpha}^*]\right\rangle + \left\langle E[v_m^{\Delta}v_{m-\alpha}^*]\right\rangle\right\}$$
$$= \frac{1}{2M^2}\sum_{\alpha=-\infty}^{\infty}h^e[\alpha]\left\{\sum_{j=0}^{M-1}\sum_{q=-\alpha M}^{(-\alpha+1)M-1}R_d(j-q)\right.$$
$$\times\sum_{l=0}^{L-1}\rho_{\xi_l}J_0(2\pi f_d\alpha T)f_l(-\varepsilon,1/2)g(-\varepsilon T_c-\tau_l)+\delta[\alpha]R_d(0)M$$
$$\left.\times\sum_{l=0}^{L-1}\rho_{\xi_l}J_0(2\pi f_d\alpha T)\sum_{\substack{i=-\infty\\ i\neq 0}}^{\infty}f_l(-i-\varepsilon,1/2)g([-i-\varepsilon]T_c-\tau_l)\right\}. \tag{B.12}$$

References

1. Borio, D., Mongrédien, C., & & Lachapelle, G. (2009). Collaborative code tracking of composite GNSS signals. *IEEE Journal of Selected Signal Processing, 3*(4), 613–626.
2. El-Tarhuni, M., & Ghrayeb, A. (2004). A robust PN code tracking algorithm for frequency selective Rayleigh-fading channels. *IEEE Transactions on Wireless Communication, 3*(4), 1018–1023.
3. Gaudenzi, R. D. (1999). Direct-sequence spread-spectrum chip tracking in the presence of unresolvable multipath components. *IEEE Transactions on Vehicular Technology, 48*(5), 1573–1583.
4. Gaudenzi, M. D., Luise, M., & Viola, R. (1993). A digital chip timing recovery loop for band-limited direct-sequence spread-spectrum signals. *IEEE Transactions on Communication, 41*(11), 1760–1769.
5. Gustafson, D. E., Dowdle, J. R., Elwell, J. M., & Flueckiger, K. W. (2009). A nonlinear code tracking filter for GPS-based navigation. *IEEE Journal of Selected Signal Processing, 3*(4), 627–638.
6. Holmes, J. K. (1982). *Coherent spread spectrum systems*. New York: Wiely.
7. Hsu, Y. -H. (2000). *Analysis of complex code tracking with channel estimation in bandlimited Rayleigh fading channels*, Master thesis, Dept. Commun. Eng., National Chiao Tung University, Hsinchu, Taiwan, July.
8. Jakes, W. C., Jr. (1974). *Microwave mobile communications*. New York: Wiely.
9. Li, H., Wang, R., & Amleh, K. (2006). Blind cod-timing estimation for CDMA systems with bandlimited chip waveforms in multipath fading channels. *IEEE Transactions on Communication, 54*(1), 141–149.
10. Ling, F. (1999). Optimum reception, performance bound, and cutoff rate analysis of references-assisted coherent CDMA communications with applications. *IEEE Transactions on Communication, 47*(10), 1583–1592.
11. Lindsey, W. C., & Simon, M. K. (1973). *Telecommunication systems engineering*, Chap. 9, Prentice-Hall.
12. Meyr, H., Moeneclaey, M., & Fechtel, S. A. (1997). *Digital communication receivers: Synchronization, channel estimation, and signal processing*. New York: Wiely.
13. Ohlson, J. E. (1978). Statistics of the first-order phase-locked loop with fluctuating signal amplitude. *IEEE Transactions on Communication, COM-26*, 1472–1474.
14. Park, H. -R. (2006). Performance analysis of a decision-feedback coherent code tracking loop for pilot-symbol-aided DS/SS system. *IEEE Transactions on Vehicular Technology, 55*(4), 1249–1258.
15. Physical Layer Standard for cdma2000 Spread Spectrum System, 3GPP2, C.S0002 Version 3.0, June 15, 2001, www.3gpp2.org.
16. Proakis, J. G. (1995). *Digital communications* (3rd ed.). New York: McGraw-Hill.
17. Sawahashi, M., Adachi, F., & Yamamoto, H. (1998). Coherent delay-locked code tracking loop using time-multiplexed pilot for DS-CDMA mobile radio. *IEICE Transactions on Communication, E81-B*(7), 1426–1432.
18. Simon, M. K., Omura, J. K., Scholtz, R. A., & Levitt, B. K. (1985). *Spread spectrum communications* (Vol. III). Rockville, MD: Computer Science Press.
19. Ueng, F. -B., Chen, J. -D., & Tsai, S. -C. (2008). Adaptive DS-CDMA receiver with code tracking in phase unknown environments. *IEEE Transactions on Wireless Communication, 7*(4), 1227–1235.
20. Van Trees, H. L. (1968). *Detection, estimation, and modulation theory—Part I*. New York: Wiely.
21. Wu, T. -M., & Tsai, T. -H. (2007). Digital code tracking loops over frequency-selective fading channels, In *Proceedings of ICC2007, ICC 2009, Glasgow, Scotland*, 24–28 June (pp. 5246–5251).

Author Biographies

Nicolas Y.-H. Hsu received the B.S. degree in electrical engineering from National Taiwan University of Science and Technology, Taipei, Taiwan in 1998. In 2000 he received the M.S. degree in communications engineering from the National Chiao Tung University, Hsinchu, Taiwan. Since 2000, he joined ASUSTeK Computer Incorporation as an R&D engineer in the Communication Software Department of the Personal Mobile Devices Business Unit.

Yu T. Su received the B.S. and Ph.D. degrees in electrical engineering from Tatung Institute of Technology, Taipei, Taiwan and the University of Southern California, Los Angeles, USA, in 1974 and 1983, respectively. From 1983 to 1989, he was with LinCom Corporation, Los Angeles, USA, where his was a Corporate Scientist involved in the design of various measurement and digital satellite communication systems. Since September 1989, he has been with the National Chiao Tung University, Hsinchu, Taiwan where he is a Professor at the Department of Electrical Engineering. He was an Associative Dean of the College of Electrical and Computer Science from 2004 to 2007, and was the Head of the Communications Engineering Department from 2001 to 2003. He is also affiliated with the Microelectronic and Information Systems Research Center of the same University and served as a Deputy Director from 1997 to 2000. From 2005 to 2008, he the Area Coordinator of Taiwan National Science Council's Telecommunications Programmer. His main research interests include communication theory and statistical signal processing.

Yuan-Bin Lin received his B.S. degree and M.S. degree in communications engineering from the National Chiao Tung University, Hsinchu, Taiwan, in 1998 and 2000, respectively. His primary research interests include all aspects of wireless communication with emphases on multiple access techniques and radio resource management. From 2003 to 2005, he was a lecturer in the Ta Hwa Institute of Technology, Hsinchu, Taiwan. In 2009 he received the Ph.D. degree in communications engineering from National Chiao Tung University, Hsinchu, Taiwan. He is currently a Post doctoral Research Fellow in the Department of Communications Engineering, National Chiao Tung University. His research interests include communication theory, radio resource management, convex optimization and cross-layer optimization for efficient transmissions on next generation wireless networks.